ISSN: 0369-8963

Mineralogical and vibrational spectroscopic insights into a carbonate–silicate pigment system in Ajanta wall paintings

M.R. Singh[1*] and Madhuri Sawant[1]

1-Department of Tourism Administration, Dr Babasaheb Ambedkar Marathwada University, Aurangabad-431004, India

- CorrespondingAuthor:M.R.Singh

Abstract

This study presents a mineralogical and spectroscopic characterization of pigment materials from 4th–5th century wall paintings of the Ajanta caves (India), integrating Raman spectroscopy, Fourier-transform infrared spectroscopy (FTIR), X-ray diffraction (XRD), and SEM–EDS microanalysis. Microscopic paint flakes obtained from deteriorated mural surfaces were first examined by reflected-light optical microscopy, revealing a stratified structure consisting of a thin pigment layer over a lime-based preparation and underlying plaster substrate. The combined analytical results indicate that the pigment assemblage is dominated by naturally occurring mineral phases, including calcite, lazurite, celadonite–glauconite, hematite–goethite, and carbon black. XRD and vibrational spectroscopic data consistently identify these phases within a carbonate-rich matrix, while SEM–EDS analysis reflects a Ca–Si–Al–Fe compositional framework characteristic of lime-supported painting systems. The absence of spectral or diffraction features attributable to modern synthetic compounds further supports the use of geogenic mineral pigments. The data indicate that the pigments are distributed within a carbonate–silicate matrix, where phase associations and microstructural relationships influence both compositional and spectroscopic responses. In particular, the dominance of calcite contributes to spectral overlap and intensity modulation in vibrational data, reflecting matrix-controlled behaviour of embedded mineral phases. These observations define a coherent carbonate–silicate pigment system characteristic of lime-based wall painting technology. The study provides mineralogical insight into phase distribution and matrix–pigment relationships in archaeological materials and establishes a reference framework for the interpretation of complex mineral assemblages in historical wall paintings.

 https://doi.org/10.5281/zenodo.20151587

ISSN: 0369-8963
Keywords: Mineral pigments; Carbonate–silicate system; Mineral assemblage; Raman spectroscopy; FTIR spectroscopy; X-ray diffraction; SEM–EDS

1. Introduction

The Ajanta caves (2nd century BCE–5th century CE), a UNESCO World Heritage monument in Maharashtra, India, preserve one of the most extensive surviving corpora of early Indian mural painting. Excavated into basalt cliffs and decorated primarily during the Vākāṭaka period (ca. 5th century CE), the murals are distinguished by complex narrative compositions, refined figural modelling, and the sophisticated use of natural mineral pigments (Figure 1A–B). Technologically, the paintings were executed using a tempera-like technique applied over a stratified plaster support composed of earthen and lime preparation layers rather than a true fresco system. This layered structure produced remarkable chromatic depth and long-term durability, features that have long attracted the attention of art historians, conservation scientists, and materials researchers interested in the composition and preservation of historical pigments (Singh & Arbad, 2014; Singh & Arbad, 2015).

Figure 1. (A) General view of the interior wall paintings and sculptural shrine of Ajanta Cave No. 2, illustrating the integration of mural decoration with architectural space. (B) Detail of a mural painting from Ajanta Cave No. 1, depicting a finely rendered female figure exemplifying the sophisticated use of natural pigments.

From a materials perspective, Ajanta represents a highly integrated painting technology in which rock-cut architecture, plaster preparation, and pigment application form a coherent technological system. The mural surfaces typically comprise a coarse earthen base derived from basaltic soil mixed with fibrous inclusions, overlaid by a fine lime-rich ground layer upon which pigments were applied (Singh & Arbad, 2015). Over nearly two millennia these surfaces

 https://doi.org/10.5281/zenodo.20151587

ISSN: 0369-8963

have been subjected to environmental exposure, localized retouching, and conservation interventions, processes that may modify the original chemical signatures of pigments and complicate their analytical interpretation (Singh & Arbad, 2013).

Because the murals are immovable and of exceptional heritage value, their investigation has relied primarily on minimally invasive sampling combined with non-destructive analytical techniques. Early studies demonstrated the applicability of spectroscopic and microanalytical approaches for identifying pigments and plaster constituents in historical wall paintings (Artioli, 2010). In recent decades, advances in archaeometric instrumentation have significantly improved the resolution of mineral phase characterization, allowing Raman spectroscopy, Fourier-transform infrared spectroscopy (FTIR), X-ray diffraction (XRD), and scanning electron microscopy coupled with energy-dispersive spectroscopy (SEM–EDS) to be integrated for the analysis of complex mineral assemblages in mural systems (Doleżyńska-Sewerniak et al., 2020; Ziemann & Madariaga, 2021).

Such multi-analytical approaches have been applied to wall paintings from diverse archaeological contexts, including Egyptian, Roman, and Byzantine monuments, where they have provided insights into pigment stratigraphy, mineral composition, and alteration processes (Guglielmi et al., 2022; Lombardi et al., 2023; Alberghina et al., 2021). In the Indian context, previous investigations have indicated that mural palettes are dominated by mineral phases such as hematite, goethite, celadonite, and glauconite, with occasional use of imported lazurite-bearing materials for blue pigments (Sharma & Singh, 2021; Sharma & Singh, 2024). These studies collectively suggest that Indian wall-painting technologies are based on lime-supported mineral systems derived from locally available geological resources.

Despite these advances, systematically integrated mineralogical datasets for the Ajanta murals remain limited. Earlier investigations have often focused on selected mural zones or conservation-related diagnostics, with limited emphasis on phase association, mineral distribution, and the interaction between pigment phases and lime-based matrices. As a result, the compositional organization of the pigment assemblage and its relationship with the carbonate-rich preparation layers remain insufficiently resolved from a mineralogical perspective.

 https://doi.org/10.5281/zenodo.20151587

ISSN: 0369-8963

The present study addresses this gap through a multi-analytical investigation of mural pigments from the Ajanta caves using Raman spectroscopy and Fourier-transform infrared spectroscopy (FTIR), supported by powder X-ray diffraction (XRD) and SEM–EDS microanalysis. The objective is to characterize the mineral phase assemblage and its distribution within a carbonate–silicate matrix by integrating molecular, crystallographic, and elemental datasets. Particular emphasis is placed on identifying phase associations and evaluating matrix–pigment relationships that influence both compositional and spectroscopic behaviour.

By adopting this integrated approach, the study moves beyond pigment identification to define a coherent mineralogical framework for Ajanta mural materials. The results provide new insight into phase organization within lime-based painting systems and establish reference data for the interpretation of complex mineral assemblages in archaeological wall paintings. In this context, the work contributes to the broader understanding of mineral-based technologies in historical mural traditions and supports future conservation and comparative archaeometric investigations.

2. Materials and Method

2.1.Sampling, Stratigraphic Examination, and Sample Preparation

Pigment microsamples were obtained from deteriorated mural surfaces in Cave 6 and Cave 11 of the Ajanta complex, both belonging to the Vākāṭaka phase (ca. 5th century CE). Sampling was restricted to naturally detached or flaking areas in order to avoid any damage to intact painted surfaces. Individual pigment flakes (<1 mm^2) representing six dominant colour groups—white (P1), blue (P2), green (P3), red (P4), yellow (P5), and black (P6)—were collected using a sterile micro-scalpel under a stereomicroscope. Samples P1–P3 were sourced from Cave 6, while P4–P6 were obtained from Cave 11.

Representative flakes were first examined under reflected-light optical microscopy to document the stratigraphy of the painting system (**Figure 2A–B**). The observations reveal a thin pigment layer applied over a lime-based preparation layer and underlying plaster substrate, consistent with established descriptions of Ajanta mural technology. This stratigraphic assessment ensured that analytical measurements targeted the pigment-bearing layer and provided essential contextual information prior to further analysis.

 https://doi.org/10.5281/zenodo.20151587

ISSN: 0369-8963

Prior to analysis, samples were briefly rinsed with analytical-grade ethanol to remove superficial contaminants. This step also aimed to reduce the potential influence of earlier conservation materials, as polyvinyl acetate (PVA) consolidants have been historically applied in parts of the Ajanta murals. Ethanol treatment was limited to rapid surface cleaning and did not involve prolonged exposure, thereby minimizing any alteration of the underlying inorganic pigment phases. As the present study focuses on mineral pigments, this treatment is not expected to affect the identification of the principal chromophoric components. No distinct organic bands attributable to consolidants were observed in the FTIR spectra, indicating that any residual conservation materials, if present, were below the detection limit of the analysis.

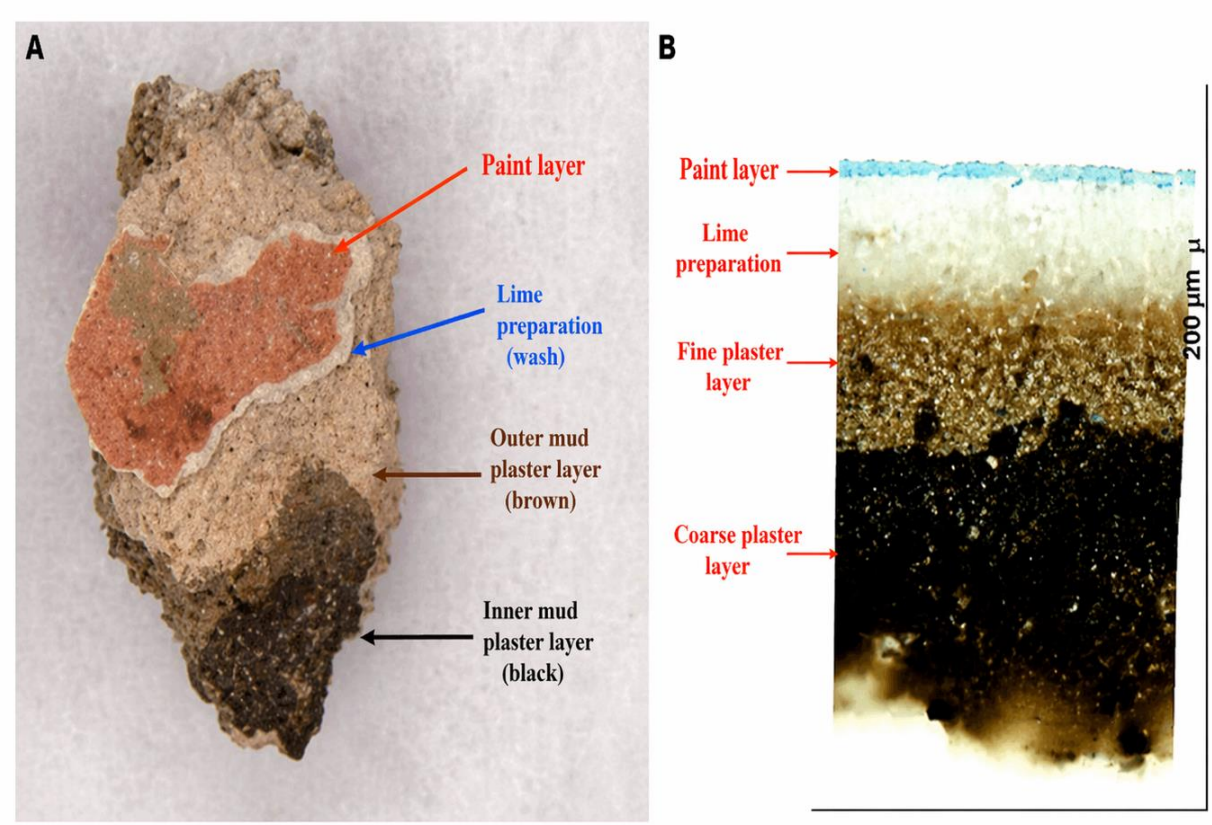

Figure 2. (A) Fragment of an Ajanta mural showing the visible stratigraphic sequence, comprising the outermost paint layer over a lime preparation (wash), followed by an outer brown mud plaster and an inner coarse black mud plaster layer. (B) Reflected-light optical cross-section of the paint fragment illustrating the multilayered structure of the mural system, including the pigment layer, lime preparation layer, fine plaster, and underlying coarse plaster. The stratigraphic observations were used to guide the selection of analytical points for Raman, FTIR, XRD, and SEM–EDS analyses.

https://doi.org/10.5281/zenodo.20151587

ISSN: 0369-8963

Following stratigraphic examination, samples were subjected to a two-stage analytical preparation. Wherever possible, analyses were performed directly on intact micro-fragments in order to preserve the spatial and compositional integrity of the pigment layer. Raman spectroscopy and SEM–EDS measurements were preferentially conducted on these unground fragments at multiple micro-spots, enabling phase-specific and elemental characterization with minimal disturbance to the original material.

A limited fraction of each sample was subsequently gently disaggregated in an agate mortar to obtain fine powders required for bulk analytical techniques. Powder preparation was restricted to analyses that necessitate homogenized material, specifically Fourier-transform infrared spectroscopy (FTIR, KBr pellet method) and X-ray diffraction (XRD), where random orientation and adequate signal intensity are essential for reliable phase identification. This combined approach allowed both micro-analytical (in situ) and bulk compositional data to be obtained from the same specimens.

All analytical measurements were performed on the same set of pigment flakes to ensure inter-technique comparability. Replicate measurements (n = 5–8 micro-spots per sample) were carried out to account for micro-scale heterogeneity. The integration of intact-fragment analysis with limited powder-based measurements provides a balanced methodology that preserves stratigraphic context while enabling robust mineralogical and microchemical characterization.The present study aims at compositional characterization of representative pigment fragments rather than statistical sampling of the entire mural corpus.

2.2 Raman Spectroscopy

Raman spectra of the six pigment samples (P1–P6) were recorded using a Horiba Xplora Plus Raman spectrometer (France) coupled with an Olympus BX optical microscope for micro-spot analysis. A 532 nm diode laser operated at low power (1–2 mW) was used to minimize thermal alteration of the pigments. The laser beam was focused through a 50× objective lens, providing a spatial resolution of approximately 1–2 μm.

Spectra were collected over the 200–1700 cm^{-1} range with a spectral resolution of 2 cm^{-1}, averaging 10–20 scans per acquisition to improve the signal-to-noise ratio. Instrument calibration was verified using the 520 cm^{-1} silicon reference band. Spectral acquisition, baseline correction, and normalization were performed using Horiba LabSpec 6 software. Vibrational bands were assigned by comparison with authenticated reference spectra available

 https://doi.org/10.5281/zenodo.20151587

ISSN: 0369-8963

in the RRUFF and IRUG pigment spectral databases, enabling reliable identification of mineral chromophores. Raman measurements were performed on intact micro-fragments at multiple micro-spots to account for heterogeneity of the pigment layer. No grinding was applied for Raman analysis in order to preserve the stratigraphic and compositional integrity of the samples.

2.3 Fourier-Transform Infrared Spectroscopy (FTIR)

FTIR measurements were performed on finely powdered pigment fractions using the KBr pellet method in the 4000–400 cm^{-1} range. The use of powdered samples allows acquisition of bulk spectral information; however, the resulting spectra may include contributions from both pigment phases and the associated lime-based matrix. Therefore, FTIR analysis was employed primarily to identify functional groups and bonding environments rather than to independently determine mineral phases.

To ensure spectral reliability, measurements were repeated on multiple sample aliquots, and only reproducible absorption bands were considered for interpretation. Spectral assignments were based on comparison with reference datasets and were cross-validated with Raman spectroscopy and XRD results.

2.4 X-Ray Diffraction (XRD)

Powder X-ray diffraction analyses were conducted using a PANalytical X'Pert PRO diffractometer equipped with Cu Kα radiation (λ = 1.5406 Å) and a graphite monochromator. Measurements were performed at an operating voltage of 40 kV and a current of 30 mA. Diffraction patterns were collected over a 2θ range of 5–80°, using a 0.02° step size and a scan rate of 1° min^{-1}.

Diffraction peaks were identified through comparison with reference patterns from the International Centre for Diffraction Data (ICDD) PDF-4+ database using PANalytical HighScore Plus software. Phase identifications were verified through comparison with Raman and FTIR results to ensure internal consistency in the mineralogical characterization of the pigment assemblage.

 https://doi.org/10.5281/zenodo.20151587

ISSN: 0369-8963

2.5 SEM–EDS Microanalysis

Elemental microanalysis of the pigment samples was performed using an Environmental Scanning Electron Microscope (ESEM, FEI Quanta 200) equipped with an Oxford Instruments INCA energy-dispersive X-ray spectrometer (EDS). Analyses were conducted in high-vacuum mode at an accelerating voltage of 20 kV, with a working distance of approximately 10 mm and a spot size of 3.5–4.0 μm.

Prior to analysis, secondary-electron (SE) and back-scattered-electron (BSE) imaging were used to locate pigment grains and examine the microstructure of the paint fragments. EDS spectra were acquired with a live time of 60–100 s to ensure adequate counting statistics.

Quantitative elemental compositions were calculated using ZAF corrections (atomic number, absorption, and fluorescence). Because the analytical volume frequently included pigment particles together with lime binder and substrate material, the results were interpreted using two complementary approaches. Raw elemental weight percentages were used to characterize the overall pigment–matrix system, while matrix-normalized compositions—excluding dominant binder elements such as O, Ca, and C—were used to emphasize the elemental signatures associated with the pigment chromophores.

For each pigment sample, multiple analytical spots (n = 5–8) were collected from the same flake to account for micro-scale heterogeneity within the paint layer. The combined analytical approach provided complementary molecular, mineralogical and elemental information for the identification of the Ajanta mural pigments.

3. Results

3.1 Raman Spectroscopic Characterization

Raman spectroscopy was employed to determine the mineralogical composition of representative pigment fragments from the Ajanta murals. Spectra were acquired over the 200–1700 cm^{-1} range using a 532 nm excitation source. Multiple spectra were collected at different micro-spots on each pigment fragment to account for micro-scale heterogeneity. Only representative spectra exhibiting clearly resolved diagnostic bands are presented (**Figure 3**), while low-intensity or noisy spectra were excluded from interpretation to avoid over-interpretation. Peak assignments were carried out through comparison with reference spectra from the RRUFF and IRUG databases and established Raman studies of mineral pigments

 https://doi.org/10.5281/zenodo.20151587

ISSN: 0369-8963

(Burgio & Clark, 2001; Smith & Clark, 2004). The principal diagnostic Raman bands and their corresponding mineral assignments are summarized in **Table 1**.

Carbonate Pigments (P1, P5)

The Raman spectrum of P1 shows two well-defined bands at approximately 712 cm^{-1} and 1085 cm^{-1}, corresponding to the ν_4 in-plane bending and ν_1 symmetric stretching modes of the carbonate group (CO_3^{2-}) in calcite ($CaCO_3$) (Sarkar, 2022). These bands represent the principal diagnostic features of calcite and confirm the presence of a lime-derived carbonate phase, as summarized in Table 1. The occurrence of calcite is consistent with its dual role as a white pigment and as a lime-based preparatory layer within the Ajanta mural system. Multiple spectra were acquired at different micro-spots for each pigment sample to account for micro-scale heterogeneity. Minor carbonate features occasionally observed in some spectra are attributed to the lime-based ground layer adhering to pigment micro-fragments rather than representing intentional pigment mixtures.

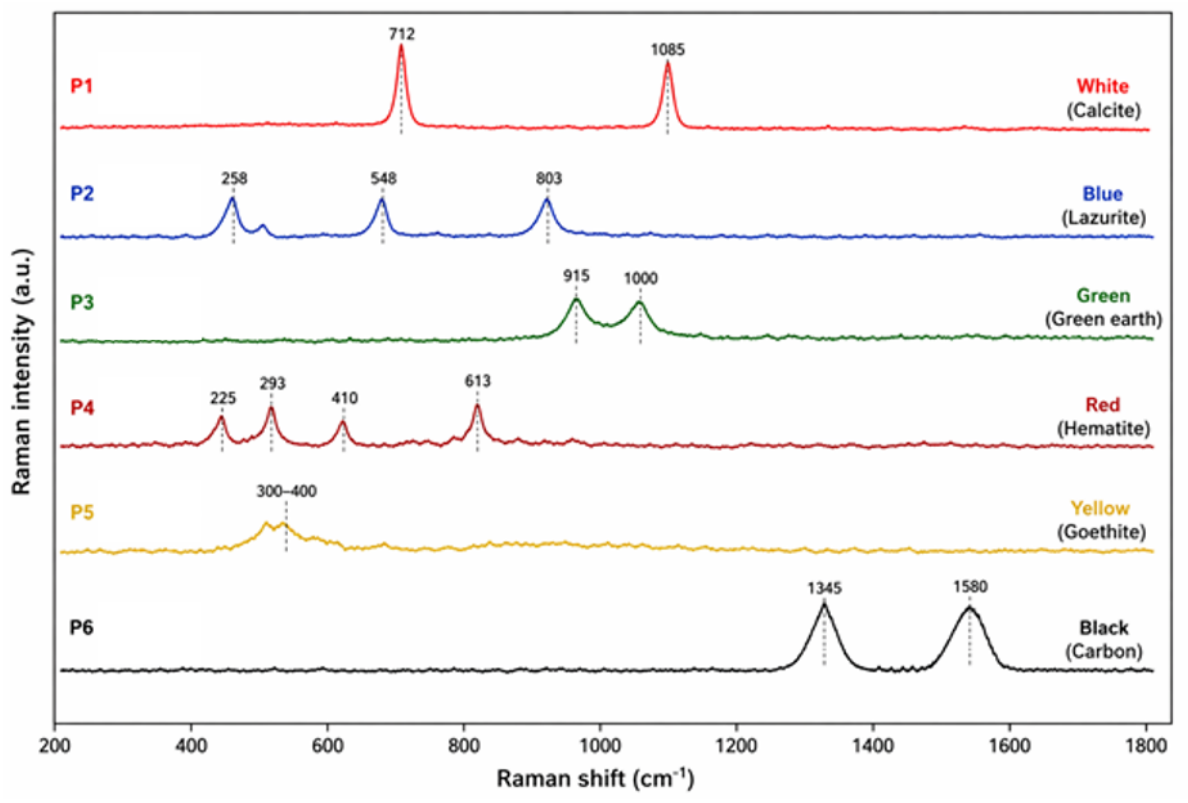

Figure 3. Raman spectra of representative pigment samples from the Ajanta murals (P1–P6), normalized over the 200–1800 cm^{-1} range. Diagnostic bands corresponding to the principal mineral pigments identified in the mural palette are indicated. Minor carbonate features

https://doi.org/10.5281/zenodo.20151587

ISSN: 0369-8963

observed in some spectra likely originate from the lime-based ground layer adhering to pigment micro-fragments.

Blue Pigment (P2)

The Raman spectrum of P2 is characterized by distinct bands at approximately 258, 548, and 803 cm^{-1}, corresponding to vibrational modes of lazurite, the chromophoric component of lapis lazuli (Bicchieri et al., 2001). The band near 548 cm^{-1}, attributed to the S_3^- radical, is the most diagnostic feature of lazurite, while bands near ~258 cm^{-1} and ~803 cm^{-1} correspond to framework vibrations of the aluminosilicate lattice. These spectral features, listed in Table 1, confirm the use of natural lapis lazuli as the blue pigment.

Green Pigment (P3)

Sample P3 exhibits bands near ~915 cm^{-1} and ~1000 cm^{-1}, along with weaker features in the lower wavenumber region. These bands correspond to Si–O stretching vibrations of Fe–Mg phyllosilicate minerals such as celadonite and glauconite (Moretto et al., 2011). The observed Raman features are consistent with green earth pigments and are summarized in Table 1.

Iron Oxide Pigments (P4-P5)

The Raman spectrum of P4 displays characteristic bands at approximately 225, 293, 410, and 613 cm^{-1}, corresponding to Fe–O lattice vibrations of hematite (α-Fe_2O_3) (Froment et al., 2008), as listed in Table 1.

The spectrum of P5 is dominated by a broad feature in the ~300–400 cm^{-1} region, consistent with goethite (α-FeOOH), indicating the presence of hydrated iron oxide phases typical of yellow ochre pigments. The absence of well-defined sharp peaks reflects the fine-grained and partially disordered nature of natural goethite, as reflected in Table 1.

Black Pigment (P6)

The Raman spectrum of P6 is characterized by two broad bands centred near ~1345 cm^{-1} and ~1580 cm^{-1}, corresponding to the D and G bands of disordered graphitic carbon (Pawlyta et al., 2015). These diagnostic features, summarized in Table 1, confirm the presence of amorphous carbon pigment.

The Raman spectra demonstrate that the pigments identified in the Ajanta samples are predominantly mineral in origin, including calcite, lazurite, green earth minerals, iron oxides (hematite and goethite), and carbon black. The assignments are based on well-defined diagnostic Raman bands (Table 1) and are consistent with reference spectra for historical pigments. Minor carbonate features occasionally observed in some spectra are attributed to the lime-based ground layer adhering to pigment micro-fragments rather than representing intentional pigment mixtures. The Raman results are corroborated by FTIR, XRD, and SEM–

 https://doi.org/10.5281/zenodo.20151587

ISSN: 0369-8963

EDS analyses, which together provide a consistent multi-analytical identification of the pigment assemblage.

Table 1. Raman spectral characteristics of pigment samples from the Ajanta murals (P1–P6). Peak positions represent mean values (±1–2 cm^{-1}) derived from replicate measurements (n = 3–5 per sample). Relative intensities are classified qualitatively as strong (s), medium (m), or weak (w). Spectral assignments were made by comparison with reference datasets from the RRUFF and IRUG databases and are supported by complementary FTIR and XRD analyses. The identification is based on well-established diagnostic Raman bands rather than minor spectral features, ensuring robust phase assignment.

Pigment colour	Mineral phase	Observed Raman bands (cm^{-1})	Relative intensity	Principal vibrational assignment	Cross-validation
White	Calcite (lime white)	**712**, **1085**, minor features near 280–285	s, s, w	ν_4 (in-plane bending) and ν_1 (symmetric stretching) modes of CO_3^{2-} in calcite	XRD (calcite reflections); FTIR carbonate bands
Red	Hematite (α-Fe_2O_3)	**225**, **293**, **410**, **613**	s, m, s, m	Fe–O lattice vibrations characteristic of crystalline hematite	XRD (hematite); FTIR Fe–O modes
Yellow	Goethite (α-FeOOH) ± hematite	**300–390**, **480–550**, weak band near 613	m, w, w	Fe–O–OH bending and lattice modes of hydrated iron oxide	XRD (goethite); FTIR hydroxyl vibrations
Green	Celadonite / Glauconite (green earth)	**~395–430**, **~550**, **~915–1000**	m, w, m	Si–O–Si and Fe–O stretching modes of Fe-Mg phyllosilicates	XRD (silicate phases); FTIR Si–O stretching
Blue	Lazurite (lapis lazuli)	**258**, **548**, **802–804**	w, s, m	S_3^- radical vibration and aluminosilicate framework modes characteristic of lazurite	XRD (lazurite phase); FTIR aluminosilicate bands

https://doi.org/10.5281/zenodo.20151587

Pigment colour	Mineral phase	Observed Raman bands (cm^{-1})	Relative intensity	Principal vibrational assignment	Cross-validation
Black	Carbon black (lamp black)	**1345**, **1580**	s, s	D and G bands of disordered graphitic carbon	XRD (amorphous phase); FTIR C=C vibrations

Note: *Minor carbonate bands occasionally observed in several spectra are attributed to the lime-based ground layer adhering to pigment micro-fragments rather than representing intentional pigment mixtures. Such substrate contributions are common in micro-fragment Raman analyses of wall paintings. Only diagnostic Raman bands are reported.*

3.2 Fourier-Transform Infrared Spectroscopy

Fourier-transform infrared (FTIR) spectroscopy was performed on six representative pigment samples (P1–P6) to identify the principal functional groups and mineral matrices associated with the Ajanta mural pigments. The spectra (**Figure 4**) exhibit characteristic absorption bands within the 4000–400 cm^{-1} range corresponding to carbonate, silicate, hydroxyl, and oxide vibrations typical of mineral pigments embedded in a lime-based matrix (Jiménez-Desmond & Pozo-Antonio, 2025; Liu & Kazarian, 2022).

Because FTIR measurements were conducted on powdered samples, the spectra represent bulk responses that may include contributions from both pigment phases and the associated preparation layer. Accordingly, FTIR results are interpreted conservatively and used as a complementary technique to Raman spectroscopy, which provides primary mineral identification. Only well-resolved and reproducible absorption bands are considered for interpretation, and the principal diagnostic features are summarized in **Table 2**.

 https://doi.org/10.5281/zenodo.20151587

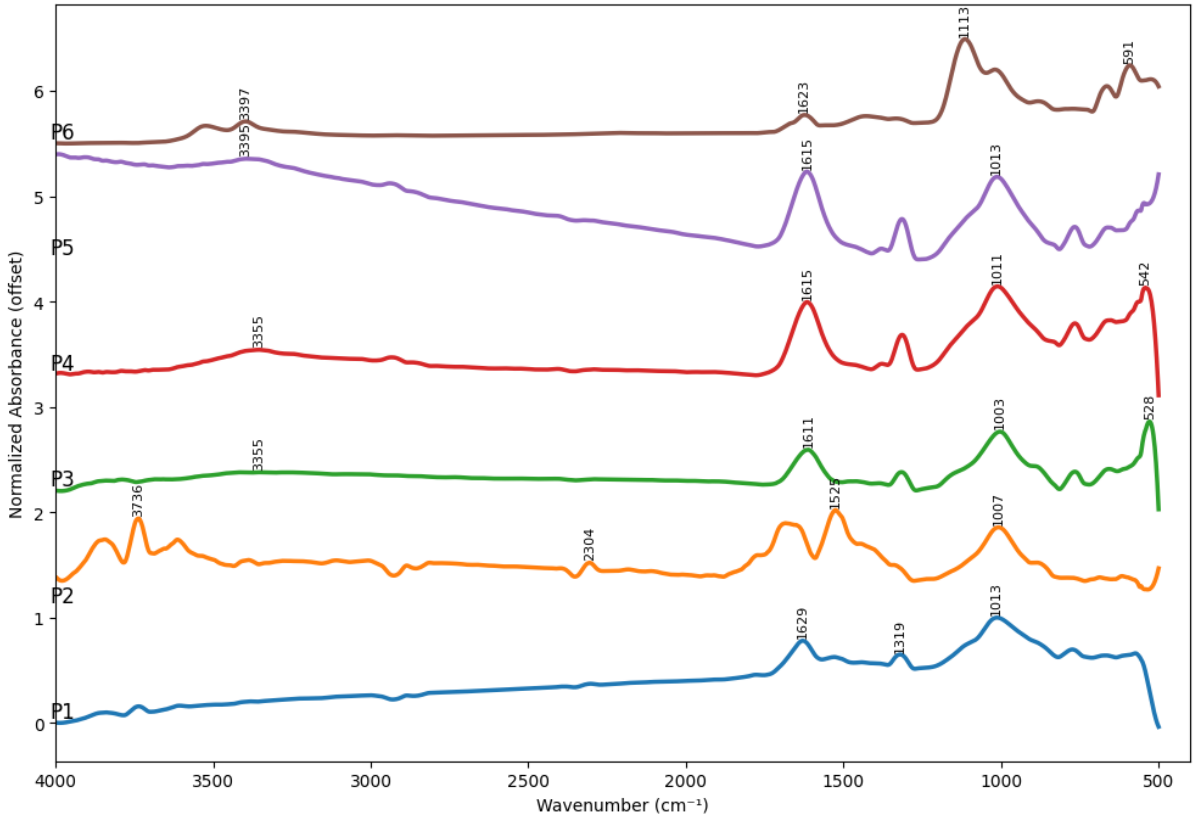

Figure 4. Stacked FTIR spectra of Ajanta pigment samples (P1–P6) plotted over the 4000–400 cm^{-1} range. Prominent absorption bands corresponding to carbonate (calcite), silicate minerals, hydroxyl groups and iron-oxide phases are indicated. Peak assignments are summarized in Table 2.

Calcite-Based White Pigments (P1, P5)

The spectra of samples P1 and P5 display prominent absorption bands at ~1420–1430, ~875, and ~712 cm^{-1}, corresponding respectively to the ν_3, ν_2, and ν_4 vibrational modes of the carbonate ion (CO_3^{2-}). These bands are characteristic of calcite ($CaCO_3$) and are clearly visible in Figure 4, with corresponding assignments listed in Table 2.

Minor absorptions in the ~3400–3600 cm^{-1} region are attributed to hydroxyl stretching vibrations associated with adsorbed moisture or alteration products commonly observed in lime-based plasters. These FTIR results support the Raman identification of calcite through its diagnostic bands at 712 and 1085 cm^{-1}, confirming the carbonate-rich matrix of the pigment and ground layer (Tankova et al., 2024).

Blue Pigment (P2)

Sample P2 exhibits absorption bands around ~1000–1020 cm^{-1} and ~560–620 cm^{-1}, corresponding to Si–O stretching and aluminosilicate framework vibrations (Figure 4; Table 2). Weak hydroxyl bands near ~3400 cm^{-1} indicate the presence of structurally bound or adsorbed water typical of aluminosilicate minerals.

 https://doi.org/10.5281/zenodo.20151587

ISSN: 0369-8963

These features are consistent with a lazurite-bearing aluminosilicate framework and support the Raman identification of lapis lazuli as the blue pigment. The absence of diagnostic carbonate or Cu–O features excludes copper carbonate pigments such as azurite or malachite, reinforcing the mineralogical assignment.

Green Pigment (P3)

The FTIR spectrum of P3 shows absorption bands near ~1000–1030 cm^{-1}, ~915 cm^{-1}, and ~520–560 cm^{-1}, corresponding to Si–O stretching, OH bending, and metal–oxygen lattice vibrations characteristic of Fe–Mg phyllosilicates (Figure 4). These features, summarized in Table 2, are consistent with celadonite and glauconite, the principal minerals of green earth pigments.

A broad OH stretching band between ~3620–3400 cm^{-1} further supports the presence of structurally bound hydroxyl groups within the phyllosilicate lattice. These results are consistent with Raman data and indicate the use of naturally occurring green earth materials.

Iron-Oxide Pigments (P4–P5)

Sample P4 exhibits a broad OH stretching band near ~3400 cm^{-1} together with weak absorptions in the ~520–560 cm^{-1} region attributable to Fe–O lattice vibrations (Figure 4; Table 2). These bands are consistent with hematite (α-Fe_2O_3) and minor goethite (α-FeOOH) present in natural ochre pigments (Volpi et al., 2023).

The relatively broad and low-intensity nature of these features reflects the fine-grained and partially disordered structure of natural iron-oxide earth pigments. The FTIR observations correspond with Raman bands observed between 225 and 613 cm^{-1}, supporting the identification of hematite–goethite assemblages.

Carbonaceous Black Pigment (P6)

The FTIR spectrum of P6 shows a largely featureless baseline typical of amorphous carbon materials (Figure 4). Weak broad bands around ~1580–1600 cm^{-1} and ~1350 cm^{-1} may correspond to aromatic C=C and C–C vibrations; however, these features are of low intensity and are interpreted cautiously. Accordingly, the identification of carbon black is based primarily on Raman spectroscopy, with FTIR providing only ancillary support.

The FTIR spectra confirm the presence of carbonate, silicate, hydroxyl, iron-oxide, and carbonaceous functional groups within the Ajanta pigment assemblage (Figure 4; Table 2). Because FTIR spectra of powdered samples inherently reflect contributions from both pigment and matrix, the technique is used here to verify functional groups rather than to independently define mineral phases. The FTIR results are consistent with Raman spectroscopy and are further supported by XRD and SEM–EDS analyses, demonstrating that the Ajanta mural

 https://doi.org/10.5281/zenodo.20151587

ISSN: 0369-8963

palette comprises calcite, lazurite, green earth minerals, iron oxides, and carbon black within a lime-based matrix (Guglielmi et al., 2020).

Table 2. FTIR spectral features of Ajanta pigment samples (P1–P6)

Colour range	Identified mineral(s)	Principal FTIR bands ($cm^{-1} \pm 2$)	Relative intensity	Vibrational assignments / Cross-validation remarks
White	Calcite	1420–1430 (s), 875 (m), 712 (s)	s / m / s	ν_3, ν_2 and ν_4 modes of CO_3^{2-}; diagnostic carbonate vibrations of calcite	Raman (712, 1085 cm^{-1}); XRD (calcite)
Blue	Lazurite (lapis lazuli)	~1000–1020 (s), 560–620 (m)	s / m	Si–O stretching and aluminosilicate framework modes consistent with lazurite; absence of Cu–O bands excludes azurite	Raman (258, 548, 802 cm^{-1}); XRD (lazurite)
Green	Celadonite / Glauconite	~1000–1030 (s), ~915 (m), ~520–560 (m)	s / m / m	Si–O stretching, OH bending and Fe–O lattice modes typical of Fe–Mg phyllosilicate green earth pigments	Raman (395–550, 915, 992 cm^{-1}); XRD (celadonite/glauconite)
Red / Yellow	Hematite ± Goethite	~520–560 (m), ~470 (w)	m / w	Fe–O stretching and Fe–O–OH bending modes associated with iron-oxide earth pigments	Raman (225–613 cm^{-1}); XRD (hematite/goethite)
Black	Carbon black	~1580 (w), ~1350 (w)	w / w	Weak aromatic C=C vibrations of amorphous carbon;	Raman (1345, 1580 cm^{-1}); SEM-EDS

https://doi.org/10.5281/zenodo.20151587

Colour range	Identified mineral(s)	Principal FTIR bands ($cm^{-1} \pm 2$)	Relative intensity	Vibrational assignments / Cross-validation remarks
				Raman provides the primary diagnostic signal

3.3 X-ray Diffraction (XRD) Analysis

Powder X-ray diffraction (XRD) analysis was performed on six representative pigment samples (P1–P6) obtained from Ajanta mural fragments. The diffraction patterns (**Figure 5**) exhibit identifiable reflections superimposed on variable background scattering, reflecting the heterogeneous mineral matrices typical of archaeological wall-painting materials. The observed peaks correspond to carbonate, silicate, and iron-oxide phases associated with the pigment assemblage.

Because the analysed samples consist of finely divided pigment fragments associated with lime-based plaster matrices, the diffraction patterns include contributions from multiple phases, and several reflections appear broadened or of moderate intensity. Accordingly, phase identification is based on diagnostic peak positions rather than minor or low-intensity features, and the principal reflections are summarized in **Table 3**. Slight smoothing was applied only for visualization purposes (Figure 5) and did not alter peak positions or relative phase interpretation. The XRD results are interpreted in conjunction with Raman and FTIR spectroscopy to ensure robust mineralogical assignment (Siddall, 2018).

 https://doi.org/10.5281/zenodo.20151587

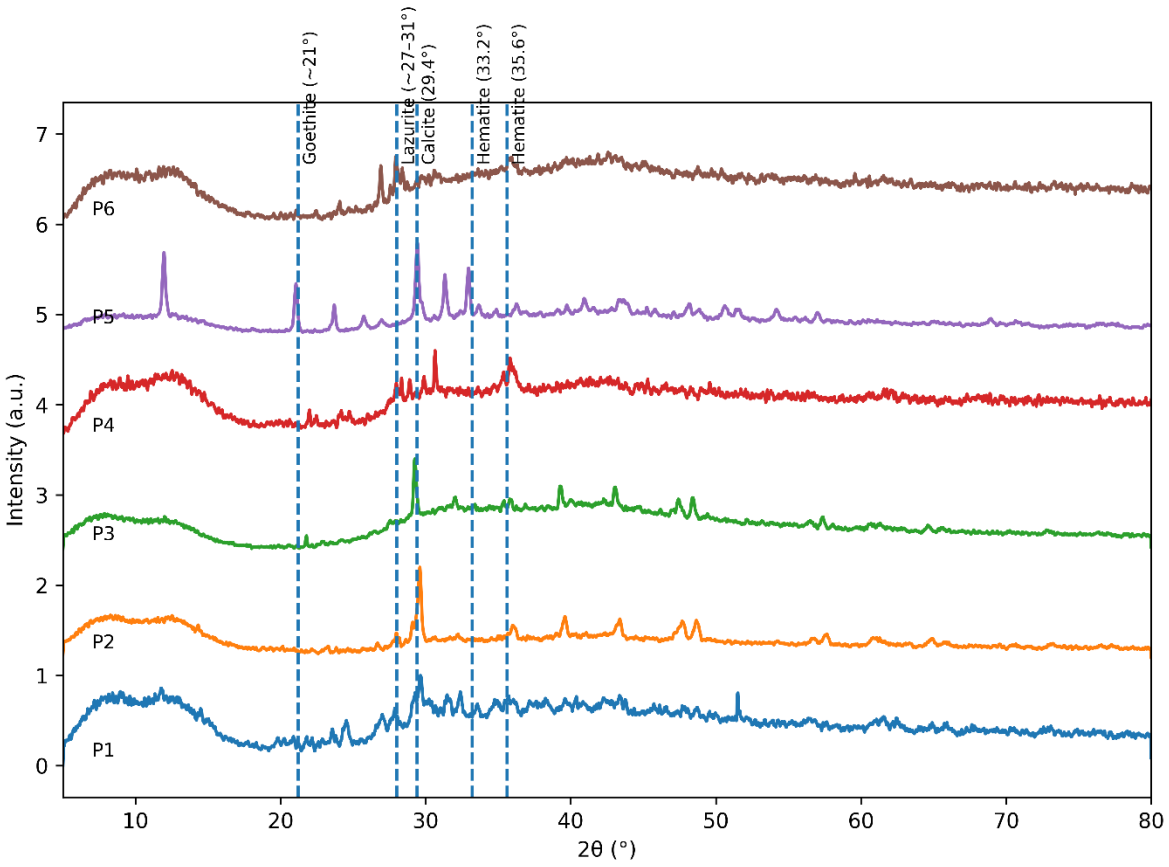

Figure 5. X-ray diffraction (XRD) patterns of Ajanta pigment samples (P1–P6) plotted over the 2θ range 5–80°. Diffraction patterns are shown with minimal smoothing applied for visualization; peak positions remain unaltered from the raw data. Major reflections corresponding to calcite, iron oxides, and silicate phases are indicated.

White Pigments (P1, P5)

Samples P1 and P5 display dominant reflections at approximately 2θ ≈ 29.4°, 39.4°, 43.1°, and 47.5°, corresponding to calcite ($CaCO_3$; PDF 05-0586), as shown in Figure 5 and summarized in Table 3. The strong reflection at 29.4° represents the principal calcite peak and confirms the presence of a carbonate phase consistent with lime-derived materials (Bearat, 2007).

Minor peak broadening is observed, reflecting fine crystallite size typical of lime-based plaster matrices. No distinct reflections attributable to sulfate minerals such as gypsum or barite were observed within the detection limits of the analysis.

Blue Pigment (P2)

The diffraction pattern of P2 shows reflections near 26.7°, 28.2°, 31.0°, 46.5°, and 50.2°, consistent with a lazurite-bearing aluminosilicate phase (Figure 5; Table 3). Given the structural complexity of natural lapis lazuli, these reflections are interpreted as representative of the aluminosilicate framework rather than as a single pure mineral phase. Minor features in

https://doi.org/10.5281/zenodo.20151587

ISSN: 0369-8963

the 22°–27° range may reflect associated silicate components; however, these are not used as primary diagnostic criteria.

The XRD data support the Raman identification of lazurite as the principal blue chromophore.

Green Pigment (P3)

Sample P3 exhibits broad reflections at approximately 2θ ≈ 20.9°, 26.4°, 35.0°, and 39.6°, consistent with Fe–Mg phyllosilicate minerals such as celadonite and glauconite (Figure 5; Table 3) (Wainwright et al., 2009).

The diffuse nature of these reflections reflects the layered structure and limited crystallinity of clay minerals. Such diffraction behaviour is typical of green earth pigments and does not allow precise phase discrimination between closely related phyllosilicate species. Therefore, the identification is based on combined XRD and Raman evidence.

Red Pigment (P4)

The diffraction pattern of P4 shows reflections at approximately 24.1°, 33.2°, 35.6°, 40.8°, and 49.5°, corresponding to hematite (α-Fe_2O_3; PDF 33-0664), as indicated in Figure 5 and Table 3. These peaks represent characteristic reflections of iron oxide pigments; however, the interpretation is restricted to the presence of hematite as the dominant phase. The absence of clear, well-resolved goethite peaks suggests that hydrated iron oxide, if present, occurs only in minor or poorly crystalline form (Perez-Rodriguez et al., 2021).

Yellow Pigment (P5)

Sample P5 exhibits reflections near 21.2°, 33.4°, 36.6°, and 53.1°, consistent with goethite (α-FeOOH), together with minor contributions from hematite (Figure 5; Table 3). The relatively broad reflections indicate fine-grain size and moderate crystallinity typical of natural ochre pigments formed through weathering processes. The coexistence of hydrated and dehydrated iron oxides is consistent with the observed yellow–brown tonal variation.

Black Pigment (P6)

The diffraction pattern of P6 shows a broad diffuse feature between approximately 20° and 30° 2θ without distinct crystalline peaks (Figure 5). This pattern is characteristic of amorphous or poorly ordered carbonaceous material and supports the presence of carbon black (Lee et al., 2021).

Because XRD is inherently insensitive to amorphous phases, this interpretation is supported primarily by Raman spectroscopy.

The XRD results (Figure 5; Table 3) indicate the presence of calcite, lazurite-bearing aluminosilicates, Fe–Mg phyllosilicates, hematite, goethite, and amorphous carbon within the analysed samples. Given the multiphase nature of the pigment–plaster system and the limited

 https://doi.org/10.5281/zenodo.20151587

ISSN: 0369-8963

sensitivity of XRD to amorphous components, phase identification is based on diagnostic reflections and cross-validation with Raman and FTIR data, rather than on exhaustive peak assignment.

No reflections corresponding to modern synthetic crystalline pigments such as titanium white, lithopone, or synthetic ultramarine were detected within the detection limits of the analysis. These results support the interpretation that the Ajanta mural palette consists predominantly of natural mineral pigments within a lime–silicate matrix, consistent with previous studies (Clerici et al., 2023; Hiley et al., 2021).

Table 3. Mineral phases identified by X-ray diffraction (XRD) and corresponding pigments in Ajanta mural samples.

Colour range	Identified mineral(s)	Diagnostic 2θ peaks (° ± 0.1)	Relative intensity / phase character	Replicates (n)	Corresponding pigment
White	Calcite	29.4, 39.4, 43.1, 47.5	Strong / well-crystalline carbonate	6	Lime white
Blue	Lazurite-bearing aluminosilicate	26.7, 28.2, 31.0, 46.5	Moderate / mixed silicate phase	6	Lapis lazuli
Green	Celadonite ± Glauconite	20.9, 26.4, 35.0, 39.6	Moderate / partially crystalline phyllosilicate	5	Green earth
Red	Hematite	33.2, 35.6, 40.8, 49.5	Strong / well-defined iron oxide	5	Red ochre
Yellow	Goethite ± Hematite	21.2, 33.4, 36.6, 53.1	Moderate / fine-grained iron oxide	5	Yellow ochre
Black	Amorphous carbon	Broad band ~20–30	Weak / diffuse scattering	6	Carbon black

Note: Values represent mean diagnostic peak positions (2θ ± 0.1°) averaged over replicate scans (n = 5–8 per pigment type). Relative intensity reflects the degree of crystallinity of the dominant phase. The approximate detection limit of the instrument is ~2 wt %. Phase

https://doi.org/10.5281/zenodo.20151587

ISSN: 0369-8963

identifications were verified through complementary Raman and FTIR spectroscopy, and instrumental calibration was confirmed using a silicon standard (2θ = 28.44°).

3.4 SEM-EDX Analysis

Point energy-dispersive X-ray spectroscopy (SEM–EDS) analyses were carried out on six representative pigment samples (P1–P6) to characterize the elemental composition of the paint layers and associated matrix (**Figure 6; Table 4**) (Ma et al., 2025; Guglielmi et al., 2022). Because the analysed volumes include pigment particles together with lime binder and clay-rich substrate, the measured spectra represent a combined pigment–matrix system rather than discrete mineral phases.

To highlight elemental associations related to the pigment phases, matrix-normalised compositions excluding dominant binder elements (O, Ca and C) were evaluated (Miriello et al., 2018). The resulting elemental patterns are interpreted in conjunction with Raman spectroscopy, FTIR analysis, and X-ray diffraction data to support mineralogical assignments.

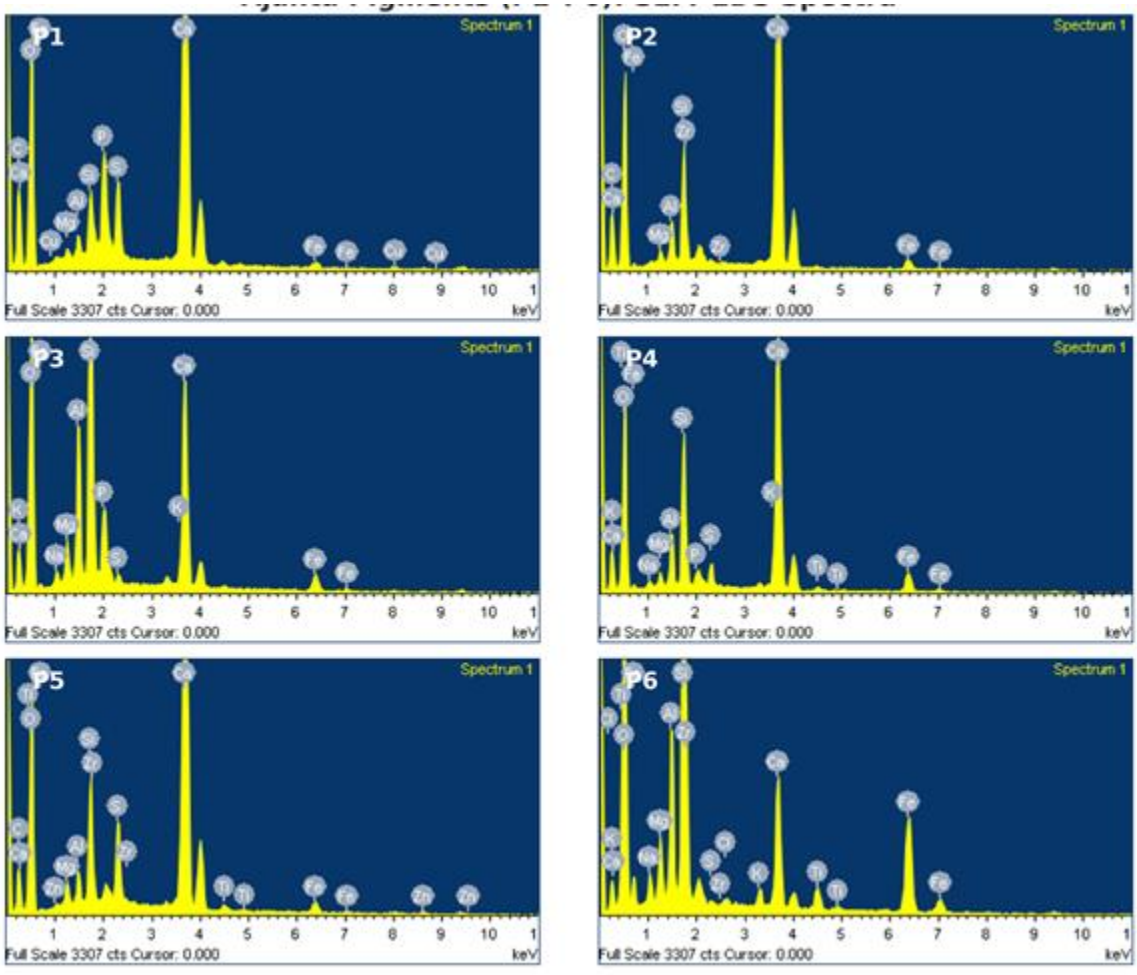

https://doi.org/10.5281/zenodo.20151587

ISSN: 0369-8963

Figure 6. Representative SEM–EDS spectra of Ajanta mural pigment samples (P1–P6). Major elemental peaks correspond to the principal mineral components of each pigment layer, including Ca from calcite (lime matrix), Si–Al–Mg–Fe from silicate and iron-oxide pigments, and trace accessory elements. The pervasive Ca and Si signals reflect the lime–silicate matrix surrounding the pigment particles.

Table 4. SEM–EDS elemental composition (wt %) of Ajanta pigment samples (P1–P6). Values represent mean ± SD derived from replicate analyses (n = 5–8 spots per sample). Data were corrected using ZAF procedures. Matrix-normalised compositions excluding dominant binder elements (O, Ca and C) were used to emphasize chromophore elements associated with the pigment phases.

Element	P1 White (mean ± SD)	P2 Blue (mean ± SD)	P3 Green (mean ± SD)	P4 Red (mean ± SD)	P5 Yellow (mean ± SD)	P6 Black (mean ± SD)
C K	14.5 ± 0.4	11.4 ± 0.3	–	–	9.1 ± 0.2	–
O K	51.5 ± 0.6	53.0 ± 0.5	58.4 ± 0.7	57.0 ± 0.6	51.7 ± 0.5	51.3 ± 0.8
Na K	–	<0.1	0.66 ± 0.05	0.82 ± 0.06	–	1.49 ± 0.07
Mg K	0.35 ± 0.03	0.62 ± 0.05	0.96 ± 0.04	1.84 ± 0.06	0.90 ± 0.04	2.13 ± 0.08
Al K	0.56 ± 0.04	1.51 ± 0.06	2.85 ± 0.09	5.76 ± 0.12	0.99 ± 0.04	4.73 ± 0.10
Si K	1.62 ± 0.08	4.36 ± 0.11	8.20 ± 0.15	15.33 ± 0.19	3.73 ± 0.09	19.23 ± 0.25
P K	2.89 ± 0.05	–	0.71 ± 0.04	3.20 ± 0.06	–	–
S K	2.58 ± 0.07	–	1.45 ± 0.06	0.57 ± 0.04	2.88 ± 0.05	0.22 ± 0.03
Cl K	–	–	–	–	–	0.26 ± 0.02
K K	–	–	0.31 ± 0.03	0.48 ± 0.04	–	0.68 ± 0.05
Ca K	24.6 ± 0.5	25.8 ± 0.6	21.9 ± 0.6	12.4 ± 0.4	27.0 ± 0.6	5.56 ± 0.18
Ti K	–	–	0.41 ± 0.03	–	0.40 ± 0.03	1.35 ± 0.07
Fe K	0.75 ± 0.05	1.59 ± 0.07	4.14 ± 0.11	2.62 ± 0.09	1.41 ± 0.06	11.09 ± 0.22
Cu K	0.55 ± 0.03	–	–	–	–	–
Zn K	–	–	–	–	0.67 ± 0.04	–
Zr L	–	1.69 ± 0.08	–	–	1.29 ± 0.06	1.95 ± 0.10

https://doi.org/10.5281/zenodo.20151587

ISSN: 0369-8963

Note: Sodium was below the detection limit in sample P2 during EDS analysis. This may result from instrumental limitations in detecting low-energy Na X-rays and from dilution by the surrounding lime matrix.

White Pigment (P1)

Ca and O dominate the EDS spectrum of the white pigment, consistent with a carbonate-rich composition. Minor amounts of S and P are detected in trace concentrations, likely reflecting sulfate phases from past restoration or environmental residues associated with lime plaster alteration. The absence of significant chromophore components supports the interpretation that the white pigment corresponds to lime-based calcite used as both a ground layer and a pigment.

Blue Pigment (P2)

The blue pigment shows a Ca-rich matrix together with detectable Si and Al, reflecting the aluminosilicate host structure surrounding lazurite grains identified by Raman and XRD.

Sodium was not detected above the analytical threshold in the EDS spectrum. This absence can be attributed to the limited sensitivity of SEM–EDS for low-energy Na Kα X-rays (~1.04 keV), combined with absorption effects and dilution within the surrounding lime matrix (Goldstein et al., 2018; Miriello et al., 2018). Similar limitations have been reported in the analysis of aluminosilicate pigments, where Na signals may be weak or below detection in spot EDS measurements (Guglielmi et al., 2022).

Green Pigment (P3)

Sample P3 exhibits a characteristic Si–Al–Mg–K elemental association with moderate Fe, typical of celadonite or glauconite, the principal minerals comprising green earth pigments. The coexistence of these elements within a lime-rich matrix is consistent with the dispersion of phyllosilicate pigment particles within the calcitic plaster binder.

Red Pigment (P4)

The red pigment shows elevated Fe together with Si and Al derived from the clay matrix. This elemental association is consistent with iron-oxide earth pigments dominated by hematite, in agreement with the Raman and XRD results. The presence of minor Al and Si reflects the clay minerals commonly associated with natural ochre deposits.

Yellow Pigment (P5)

The yellow pigment exhibits Fe together with minor Ti and S, consistent with goethite-bearing ochre pigments containing small amounts of accessory minerals. Trace Zn and Zr detected in this sample are interpreted as minor accessory phases or environmental particulates incorporated into the paint layer.

 https://doi.org/10.5281/zenodo.20151587

ISSN: 0369-8963

Black Pigment (P6)

The EDS spectrum of the black pigment displays a residual Si–Fe–Al signal derived from the surrounding silicate matrix. Carbon cannot be reliably quantified under carbon coating conditions; however, the absence of diagnostic metal chromophores, together with Raman identification, supports the interpretation of amorphous carbon black used for outlines and shading.

The SEM–EDS data indicate that the Ajanta pigments are embedded within a lime–silicate matrix supporting mineral chromophores, including calcite, lazurite, celadonite/glauconite, hematite, goethite, and carbonaceous material. Variations in elemental abundances primarily reflect differences in pigment-to-binder ratios and the heterogeneous nature of the paint layers rather than distinct compositional technologies. When interpreted together with Raman spectroscopy, FTIR analysis, and X-ray diffraction results, the EDS data provide consistent elemental support for the mineral pigment assemblage identified in the Ajanta murals (Irazola et al., 2012; Guglielmi et al., 2022).

4. Discussion

The analytical investigation undertaken in this study provides an integrated reconstruction of the mineral assemblage and phase organization of pigment materials employed in the Ajanta murals. The convergence of molecular, crystallographic, and elemental datasets indicates that the mural palette is composed of a well-defined suite of mineral phases—calcite, lazurite, celadonite–glauconite, hematite–goethite, and carbon black—forming a coherent pigment assemblage within a carbonate-rich matrix. These phases reflect a stable mineral system in which optical and physicochemical properties are closely linked to their distribution within lime-based substrates.

Raman spectroscopy provides diagnostic fingerprints of the constituent mineral phases, enabling the identification of carbonate, aluminosilicate, iron-oxide, and carbonaceous components. These observations are supported by FTIR spectra, which reflect the associated functional groups related to carbonate, silicate, hydroxyl, and oxide vibrations. The complementarity between Raman and FTIR techniques is well established in archaeometric studies of wall paintings, where Raman spectroscopy is effective for phase identification, while FTIR provides insight into bonding environments and matrix-related contributions (Casadio et al., 2016; Liu & Kazarian, 2022). Recent developments in Raman spectral libraries further support the reproducibility of mineral phase identification in heritage materials (Innocenti et al., 2024).

 https://doi.org/10.5281/zenodo.20151587

ISSN: 0369-8963

Beyond phase identification, the combined vibrational dataset reflects the influence of the surrounding carbonate matrix on spectral behaviour. The dominance of calcite-related bands in FTIR spectra, together with their overlap with silicate and hydroxyl vibrations, indicates that the spectral response of pigment phases is modulated by the calcitic environment. Similarly, variations in Raman band intensity and relative prominence among samples can be attributed to differences in phase abundance, grain size, and matrix interactions. These observations indicate that vibrational responses in such systems are governed not only by intrinsic mineral signatures but also by matrix-controlled effects, highlighting the importance of considering pigment–matrix interactions in the interpretation of complex mineral assemblages.

The X-ray diffraction results further support these interpretations by identifying crystalline phases consistent with calcite, lazurite-bearing aluminosilicates, celadonite/glauconite, hematite, and goethite. The relatively diffuse diffraction features observed in several samples reflect the fine-grained and heterogeneous nature of archaeological paint layers, in which pigment crystallites are dispersed within lime plaster and clay-rich matrices. Comparable diffraction characteristics have been reported in historical wall painting materials where mineral phases are intimately associated with plaster substrates and alteration products (Siddall, 2018). The absence of reflections corresponding to modern synthetic compounds—such as ultramarine, titanium white, or lithopone—further indicates that the assemblage is dominated by naturally occurring mineral phases.

Elemental data obtained through SEM–EDS analysis provide complementary insight into the microchemical framework of the pigment layers. The spectra indicate a calcium-rich matrix associated with lime plaster, together with variable proportions of silicon, aluminium, iron, and magnesium corresponding to silicate and iron-oxide phases. This elemental distribution reflects a carbonate–silicate–oxide system in which mineral pigments are embedded within a calcitic binder derived from calcined limestone. Such mineralogical associations are characteristic of lime-supported painting techniques widely employed in ancient mural traditions, where pigments were applied onto prepared substrates rather than incorporated into wet plaster layers, as in true fresco techniques (Artioli, 2010).

The identification of lazurite as the blue pigment is particularly significant from a mineralogical perspective. Lapis lazuli, containing lazurite as its principal chromophoric phase, is a non-local material historically sourced from deposits in Afghanistan and Central Asia. Its occurrence within the Ajanta murals suggests long-distance material transfer and selective incorporation of high-value mineral resources (Sharma & Singh, 2024). The coexistence of lazurite with locally available iron oxides and green earth minerals reflects a composite mineral assemblage

 https://doi.org/10.5281/zenodo.20151587

ISSN: 0369-8963

combining regional geological materials with imported phases to achieve specific chromatic and visual effects.

Equally important is the role of the carbonate matrix in stabilizing the pigment assemblage. The consistent presence of calcite across multiple analytical techniques indicates that lime-based preparation layers functioned not only as a structural substrate but also as a chemically compatible matrix facilitating pigment dispersion and long-term preservation. The interaction between carbonate binders and silicate or iron-oxide phases contributes to the stability of the mineral assemblage under varying environmental conditions. From a vibrational perspective, this carbonate-rich matrix governs the spectral response of embedded phases through band overlap, intensity variation, and matrix-related spectral contributions.

Taken together, the analytical evidence indicates that the Ajanta murals represent a well-organized carbonate–silicate mineral system derived from empirical knowledge of locally available geological resources and selective material acquisition. The pigment assemblage—comprising carbonate binders, aluminosilicate minerals, iron oxides, and carbonaceous phases—forms a chemically coherent system consistent with mineral-based technologies documented in other ancient mural traditions across the Mediterranean and Asia (Guglielmi et al., 2022; Lombardi et al., 2023).

Beyond compositional identification, the present dataset provides insight into the organization and behaviour of mineral phases within a lime-based matrix. The results indicate that pigment performance and preservation are closely linked to phase distribution and matrix–pigment relationships, which control both structural stability and spectroscopic response. This integrated approach demonstrates that the interpretation of archaeological pigment systems requires consideration of mineral assemblages as interacting systems rather than isolated components, thereby reinforcing the importance of multi-analytical frameworks for resolving complex mineralogical materials.

Conclusion

This study provides an integrated mineralogical assessment of the pigment system of the Ajanta murals through the combined application of Raman spectroscopy, FTIR spectroscopy, X-ray diffraction, and SEM–EDS microanalysis. The analytical results indicate that the mural palette is dominated by a coherent assemblage of mineral phases—including calcite, lazurite, celadonite, glauconite, hematite, goethite, and carbon black—distributed within a lime-rich preparation layer. The consistent association of carbonate binders with silicate and iron-oxide phases defines a stable carbonate–silicate system, in which mineral compatibility likely contributed to the long-term preservation of the mural surfaces. The occurrence of lazurite

 https://doi.org/10.5281/zenodo.20151587

further indicates the selective incorporation of imported mineral materials alongside locally available earth pigments, reflecting a structured and resource-informed approach to pigment selection. Beyond compositional identification, the results indicate that the carbonate-rich matrix exerts a controlling influence on the behaviour of the pigment assemblage, affecting both phase distribution and vibrational response through band overlap, intensity variation, and matrix-related spectral contributions. These observations highlight the importance of considering mineral–matrix relationships when interpreting vibrational data from complex wall-painting systems. By integrating molecular, crystallographic, and elemental datasets, this study establishes a mineralogically grounded framework for the characterization of pigment systems in lime-based painting materials and provides reference data for the analysis of complex mineral assemblages in archaeological wall paintings.

Acknowledgements:

The authors are grateful to the Department of Physics and CRAFT section of Dr. Babasaheb Ambedkar Marathwada University, Chhatrapati Sambhajinagar for all the help extended in the analysis of the pigment samples.

Data Availability Statement

All the data generated in this study has been incorporated in the manuscript and may be provided by the corresponding author on reasonable request.

Funding Statement:

The authors declare that no funding was received for this manuscript

Conflict of Interest

The authors declare no conflict of interest technical or financial.

Consent to Publish

All the authors have given their consent to publish this manuscript.

Ethical Statement

Not applicable

Authors Contribution:

Certified that all the authors have contributed equally for this manuscript.

References

Alberghina, M. F., Milazzo, G., Schiavone, S., Randazzo, L., Ricca, M., Rovella, N., ... & La Russa, M. F. (2021). The contribution of microchemical analyses and diagnostic imaging to the conservation and identification of the degraded surfaces of hellenistic-roman wall paintings

from Solunto (Sicily). *Studies in Conservation*, *66*(6), 342-356. https://doi.org/10.1080/00393630.2020.1805252

Artioli, D., Capanna, F., Giovagnoli, A., Ioele, M., Marcone, A., Mariottini, M., ... & Singh, M. (2008, May). Mural paintings of Ajanta Caves, part II: Non destructive investigations and microanalysis on execution technique and state of conservation. In *Conf. NDT Art, Jerusalem Isr* (pp. 25-30). www.ndt.net/search/docs.php3?MainSource=65

Artioli, G. (2010). *Scientific methods and cultural heritage: an introduction to the application of materials science to archaeometry and conservation science*. OUP Oxford. ISBN:9780191576355, 0191576352

Astolfi, M. L. (2023). Advances in analytical strategies to study cultural heritage samples. *Molecules*, *28*(17), 6423. **https://doi.org/10.3390/molecules28176423**

Avranovich Clerici, E., De Meyer, S., Vanmeert, F., Legrand, S., Monico, L., Miliani, C., & Janssens, K. (2023). Multi-scale X-ray imaging of the pigment discoloration processes triggered by chlorine compounds in the upper Basilica of Saint Francis of Assisi. *Molecules*, *28*(16), 6106. **https://doi.org/10.3390/molecules28166106**

Béarat, H. (1996). Chemical and mineralogical analyses of Gallo-Roman wall painting from Dietikon, Switzerland. *Archaeometry*, *38*(1), 81-95. **https://doi.org/10.1111/j.1475-4754.1996.tb00762.x**

Bicchieri, M., Nardone, M., Russo, P. A., Sodo, A., Corsi, M., Cristoforetti, G., ... & Tognoni, E. (2001). Characterization of azurite and lazurite based pigments by laser induced breakdown spectroscopy and micro-Raman spectroscopy. *Spectrochimica Acta Part B: Atomic Spectroscopy*, *56*(6), 915-922. https://doi.org/10.1016/S0584-8547(01)00228-2

Burgio, L., & Clark, R. J. H. (2001). Library of FT-Raman spectra of pigments, minerals, pigment media and varnishes, and supplement to existing libraries. Spectrochimica Acta Part A: Molecular and Biomolecular Spectroscopy, 57(7), 1491–1521. https://doi.org/10.1016/S1386-1425(00)00495-9

Casadio, F., Daher, C., & Bellot-Gurlet, L. (2016). Raman spectroscopy of cultural heritage materials: overview of applications and new frontiers in instrumentation, sampling modalities, and data processing. *Analytical chemistry for cultural heritage*, 161-211. https://doi.org/10.1007/978-3-319-52804-5_5

Doleżyńska-Sewerniak, E., Jendrzejewski, R., Klisińska-Kopacz, A., & Sawczak, M. (2020). Non-invasive spectroscopic methods for the identification of drawing materials used in XVIII century. *Journal of Cultural Heritage*, *41*, 34-42. https://doi.org/10.1016/j.culher.2019.07.008

Fioretti, G., Tempesta, G., Capotorto, S., & Eramo, G. (2023). Non-Invasive Characterisation of the Wall Paintings in the Byzantine Church of Palazzo Simi (Bari, Italy) and Digital Photogrammetric Survey for a Pigment Mapping. *Coatings*, *13*(6), 996. **https://doi.org/10.3390/coatings13060996**

Froment, F., Tournié, A., & Colomban, P. (2008). Raman identification of natural red to yellow pigments: ochre and iron-containing ores. *Journal of Raman Spectroscopy: An International Journal for Original Work in all Aspects of Raman Spectroscopy, Including Higher Order Processes, and also Brillouin and Rayleigh Scattering*, *39*(5), 560-568. **https://doi.org/10.1002/jrs.1858**

Giovagnoli, A., Capanna, F., Ioele, M., Marcone, A. M., Ozino-Caligaris, E., Risotto, L., & Singh, M. (2008). The mural paintings of the ajanta caves, part I: documentation on execution techniques and conservation condition. *Art 2008-Non-destructive investigations and microanalysis for the diagnostics and conservation of cultural and environmental heritage*. www.ndt.net/search/docs.php3?MainSource=65

Goldstein, J. I., Newbury, D. E., Michael, J. R., Ritchie, N. W., Scott, J. H. J., & Joy, D. C. (2017). *Scanning electron microscopy and X-ray microanalysis*. springer. ISBN: 9781493966769, 1493966766

Guglielmi, V., Andreoli, M., Comite, V., Baroni, A., & Fermo, P. (2022). The combined use of SEM-EDX, Raman, ATR-FTIR and visible reflectance techniques for the characterisation of Roman wall painting pigments from Monte d'Oro area (Rome): An insight into red, yellow and pink shades. *Environmental Science and Pollution Research*, *29*(20), 29419-29437. https://doi.org/10.1007/s11356-021-15085-w

Guglielmi, V., Comite, V., Andreoli, M., Demartin, F., Lombardi, C. A., & Fermo, P. (2020). Pigments on Roman wall painting and stucco fragments from the Monte d'Oro Area (Rome): a multi-technique approach. *Applied Sciences*, *10*(20), 7121. **https://doi.org/10.3390/app10207121**

Guglielmi, V., Andreotti, A., & Colombini, M. P. (2022). Multi-analytical characterization of pigments in cultural heritage materials. Microchemical Journal, 176, 107239. https://doi.org/10.1016/j.microc.2022.107239

Gupta, D., Singh, M., & Sawant, M. (2025). From murals to microclimate: assessing the ecological footprint of tourism at Ajanta Caves. *Journal of Heritage Tourism*, *20*(2), 260-281. https://doi.org/10.1080/1743873X.2024.2419041

Hiley, C. I., Hansford, G., & Eastaugh, N. (2022). High-resolution non-invasive X-ray diffraction analysis of artists' paints. *Journal of Cultural Heritage*, *53*, 1-13. https://doi.org/10.1016/j.culher.2021.10.008

Innocenti, S., Quintero Balbas, D., Galeotti, M., Cagnini, A., Porcinai, S., & Striova, J. (2024). Historical pigments and paint layers: Raman spectral library with 852 nm excitation laser. *Minerals*, *14*(6), 557. **https://doi.org/10.3390/min14060557**

Irazola, M., Olivares, M., Castro, K., Maguregui, M., Martínez-Arkarazo, I., & Madariaga, J. M. (2012). In situ Raman spectroscopy analysis combined with Raman and SEM-EDS imaging to assess the conservation state of 16th century wall paintings. *Journal of Raman Spectroscopy*, *43*(11), 1676-1684. **https://doi.org/10.1002/jrs.4036**

Jiménez-Desmond, D., & Pozo-Antonio, J. S. (2025). Fourier transform infrared (FTIR) database of historical pigments: a comparison between ATR-FTIR and DRIFT modalities. *Applied Sciences*, *15*(7), 3941. **https://doi.org/10.3390/app15073941**

Lee, S. M., Lee, S. H., & Roh, J. S. (2021). Analysis of activation process of carbon black based on structural parameters obtained by XRD analysis. *Crystals*, *11*(2), 153. **https://doi.org/10.3390/cryst11020153**

Liu, G. L., & Kazarian, S. G. (2022). Recent advances and applications to cultural heritage using ATR-FTIR spectroscopy and ATR-FTIR spectroscopic imaging. *Analyst*, *147*(9), 1777-1797. DOI: 10.1039/D2AN00005A

Lombardi, C. A., Comite, V., Fermo, P., Bergomi, A., Trombino, L., & Guglielmi, V. (2023). A multi-analytical approach for the characterisation of pigments from an Egyptian sarcophagus cover of the late dynastic period: a case study. *Sustainability*, *15*(3), 2002. **https://doi.org/10.3390/su15032002**

Lombardo, T., Caroselli, M., Martinucci, C., Hildbrand, E., Moretti, P., & Cassitti, P. (2024). Exploring Carolingian and Romanesque cycles: a study of the detached wall paintings from the Church of St. Johann in Müstair. *Heritage Science*, *12*(1), 347. https://doi.org/10.1186/s40494-024-01465-1

Ma, C., Dou, H., Zhao, Z., Qiu, X., Li, H., & Wang, X. (2025). Review of in-situ non-and micro-destructive techniques for pigment analysis in architectural heritage. *npj Heritage Science*, *13*(1), 222. https://doi.org/10.1038/s40494-025-01675-1

Miriello, D., Bloise, A., Crisci, G. M., De Luca, R., De Nigris, B., Martellone, A., ... & Ruggieri, N. (2018). Non-destructive multi-analytical approach to study the pigments of wall painting fragments reused in mortars from the archaeological site of Pompeii (Italy). *Minerals*, *8*(4), 134. **https://doi.org/10.3390/min8040134**

Moretto, L. M., Orsega, E. F., & Mazzocchin, G. A. (2011). Spectroscopic methods for the analysis of celadonite and glauconite in Roman green wall paintings. *Journal of Cultural Heritage*, *12*(4), 384-391. https://doi.org/10.1016/j.culher.2011.04.003

Pawlyta, M., Rouzaud, J. N., & Duber, S. (2015). Raman micro spectroscopy characterization of carbon blacks: Spectral analysis and structural information. *Carbon*, *84*, 479-490. https://doi.org/10.1016/j.carbon.2014.12.030

Perez-Rodriguez, J. L., Franquelo, M. L., & Duran, A. (2021). TG, DTA and X-ray thermodiffraction study of wall paintings from the fifteenth century. *Journal of Thermal Analysis & Calorimetry*, *143*(4). **DOI: 10.1007/s10973-020-09420-5**

Possenti, E., Miliani, C., Cotte, M., Realini, M., & Colombo, C. (2025). SR-based μXRD–μXRF 2D mapping to study Mg-rich historical frescoes subjected to inorganic conservation treatments. *Analyst*, *150*(8), 1590-1604. DOI: 10.1039/D4AN01548G

Sarkar, C. G. (2022). Pigments in Ancient Manuscripts and Paintings Brought to Life by Raman Spectroscopy-A Short Review. *Oriental Journal of Chemistry*, *38*(5), 1081. DOI:10.13005/ojc/380501

Sharma, A. and Singh M.R. (2024). Historical Blue Pigments Used in India's Wall Paintings-A Review. *Cultural Arts Research and Development*, *4*(2), 24-42. https://doi.org/10.55121/card.v4i2.228

Sharma, A., & Singh, M. R. (2021). A Review on Historical Earth Pigments Used in India's Wall Paintings. *Heritage*, *4*(3), 1970-1994. **https: /doi.org/10.3390/heritage4030112**

Shimadzu, Y. (2021). Painting Materials and Techniques of the Ajanta Wall Paintings. *Conservation and Painting Techniques of Wall Paintings on the Ancient Silk Road*, 137-156. https://doi.org/10.1007/978-981-33-4161-6_8

Siddall, R. (2018). *Mineral pigments in archaeology: their analysis and the range of available materials Minerals, 8 (5), 201*. **https://doi.org/10.3390/min8050201**

Singh M.R. and ARBAD, B. (2013). CHEMISTRY OF PRESERVATION OF THE AJANTA MURALS. *International Journal of Conservation Science*, *4*(2). **ISSN 2067-533X**

Singh M.R. and Arbad, B. R. (2014). ANCIENT INDIAN PAINTING RECIPES AND MURAL ART TECHNIQUE AT AJANTA. *International Journal of Conservation Science*, *5*(1). **ISSN 2067-533X**

Singh, M., & Arbad, B. R. (2015). Characterization of 4th–5th century AD earthen plaster support layers of Ajanta mural paintings. *Construction and Building materials*, *82*, 142-154. https://doi.org/10.1016/j.conbuildmat.2015.02.043

Singh, M., Gupta, D. A., & Sawant, D. M. (2024). Assessing the carrying capacity for the environmental protection of the ancient artworks of India's Ajanta caves. *Tourism Review*. https://doi.org/10.1108/TR-11-2023-0791

Smith, G. D., & Clark, R. J. H. (2004). Raman microscopy in art history and conservation science. Reviews in Conservation, 5, 92–106. https://doi.org/10.1179/sic.2004.49.Supplement-1.92

Tankova, V., Atanassova, V., Mihailov, V., & Pirovska, A. (2024). Spectroscopic Identification of Mineral Pigments in White Decorated Prehistoric Pottery from Bulgaria. *Minerals*, *14*(7), 683. **https://doi.org/10.3390/min14070683**

Volpi, F., Vagnini, M., Vivani, R., Malagodi, M., & Fiocco, G. (2023). Non-invasive identification of red and yellow oxide and sulfide pigments in wall-paintings with portable ER-FTIR spectroscopy. *Journal of Cultural Heritage*, *63*, 158-168. https://doi.org/10.1016/j.culher.2023.07.019

Wainwright, I. N., Moffatt, E. A., & Sirois, P. J. (2009). Occurrences of green earth pigment on Northwest Coast first nations painted objects. *Archaeometry*, *51*(3), 440-456. **https://doi.org/10.1111/j.1475-4754.2008.00410.x**

Ziemann, M. A., & Madariaga, J. M. (2021). Applications of Raman spectroscopy in art and archaeology. *J. Raman Spectrosc*, *52*(1), 8-14. DOI: 10.1002/jrs.6054